In situ reduction of Ag on magnetic nanoparticles with gallic acid: effect of the synthesis parameters on morphology

In situ reduction of Ag on magnetic nanoparticles with gallic acid: effect of the synthesis parameters on morphology

Abstract

Fe_3O_4—Ag composite nanoparticles (NPs) were prepared by a new *in situ* reduction of Ag on the surface of Fe_3O_4 NPs using gallic acid as reducing agent in different NPs/gallic acid ratio. The obtained NPs were characterized by Field-Emission Scanning/Scanning Transmission Electron Microscopy and Fourier-transform infrared spectroscopy in order to evaluate their crystal structure, their morphology, the effective functionalization and the presence of Ag. Different morphologies were obtained: polydispersed aggregates, nanoflower-like and nanodumbbell nanocomposites, depending on the synthesis conditions. Well-defined Fe_3O_4-Ag nanodumbbells were obtained in aqueous media, with NPs/gallic acid ratio of 10:1. It was also assessed that silica shell is not a key issue to optimize the morphology of Ag NPs nucleated on the Fe_3O_4 core.

Structured Abstract

Aim: Synthesis of Fe_3O_4—Ag composite nanoparticles by a new *in situ* reduction of Ag NPs on the surface of Fe_3O_4 NPs using gallic acid as reducing agent.

Materials & Methods: The influence of process parameters on NPs morphology and functionalization was evaluated by means Field-Emission Scanning/Scanning Transmission Electron Microscopy and Fourier-transform infrared spectroscopy.

Results and Conclusions: The synthesis conditions affect the morphology of the obtained nanoparticles, evidencing the formation of polydispersed aggregates, nanoflower-like or nanodumbbell nanocomposites. In particular, well-defined

nanodumbbells were obtained in aqueous media, with NPs/gallic acid ratio of 10:1; while the presence of a silica shell did not improve the morphology of Ag NPs nucleated on the Fe_3O_4 core.

Lay abstract:

Nanoparticles (NPs) are extensively investigated in the biomedical field for the diagnosis and the treatment of tumors. The aim of this work is to develop a simple and green method to produce composite nanoparticles, formed by iron oxides (magnetic) and silver NPs. Magnetic NPs can be moved using an external magnetic field and localized in the tumor; silver NPs can generate useful heat to kill tumor cells when exposed to light and possess antibacterial properties. The performed study showed that by varying the process parameters (e.g. amount of reagents, presence of coatings on the particles ...), it is possible to obtain multifunctional NPs with different shapes and sizes, potentially useful for the treatment of tumors.

Keywords

Magnetic nanoparticles, silver nanoparticles, *in situ* reduction, gallic acid.

Introduction

Magnetic nanoparticles (MNPs) are one of main objects of study in the current literature concerning nanotechnology [1, 2]. MNPs are often suggested in biomedical applications as drug carriers due to their ability, when exposed to an external magnetic field, to be moved purposely to a target site in the human body. Most of the MNPs described in literature are composed of iron oxide (mainly Fe_3O_4 or γ-Fe_2O_3) often used as magnetic

cores enclosed into an organic or inorganic shell (such as silica, gold, fatty acid, citric acid and others) [3-5]. Iron oxide MNPs are among the most appropriate nanoplatforms for biomedical applications due to their chemical stability, superparamagnetism, biocompatibility, easiness of synthesis and since they can be further functionalized with molecules of particular interest, such as anticancer drug or specific bioactive molecules [3-5]. Iron oxide MNPs are used as contrast agents in magnetic resonance imagining (MRI), drug delivery systems [6, 7] and deeply investigated for applications in the field of cancer treatment by hyperthermia [2, 8, 9].

The decoration of the magnetic core with ultra-small metal nanoparticles can further enhance the variety of potential applications of this versatile category of nanoplatform in biomedical field, merging the magnetic properties of the core with the peculiar properties of metal nanoparticles [10, 11].

For example, silver nanoparticles are of great interest because they exhibit peculiar functionalities, such as, among others, antimicrobial, antiviral, optical and catalytic properties [12-15]. Their chemical stability, biocompatibility and long-term efficacy toward a broad bacterial spectrum make them suitable in many biomedical applications as targeted tool for *in situ* infection treatment [16].

Besides the well-known antimicrobial activity [14, 17, 18], silver nanoparticles are of great interest in the field of surface-enhanced Raman spectroscopy [19] and photothermal cancer therapy [20]. Silver nanoparticles exhibit strong absorption band at about 400 nm. The position of the absorption band can vary depending on the size and shape of silver nanoparticles.

Magnetic iron oxide nanoparticles and silver nanoparticles can be combined into nanocomposite platforms implementing the above mentioned properties [6]. For example,

the decoration of Fe_3O_4 nanoparticles with Ag nanoparticles gives rise to enhanced optical responses [21]. Moreover, the combination of magnetic (Fe_3O_4) and antibacterial (Ag) properties, can be exploited for the magnetic targeting and removal of antimicrobial agent.

Since magnetic nanoparticles are very sensitive to agglomeration, many methods have been investigated in literature to impart electrostatic or steric repulsion, such as the coating with organic (e.g. surfactants, polymers) or inorganic materials (e.g. silica, metal oxides, metals) [22, 23]. Moreover, MNPs have been decorated with noble metals NPs, especially Au NPs, by using different approaches [24]. One of the proposed methods to decorate MNPs with metallic NPs is to cover the magnetic NPs with a silica layer, which can be easy functionalized and acts as intermediate layer between the magnetic core and the metallic NPs [25]. Noble metal NPs can be also directly attached to the magnetic core using silanes or coupling and reducing agents such as $NaBH_4$, hydroxylamine, plant extracts, or by the metal NPs adsorption on magnetic NPs surface [11, 24, 26-30].

In the present work we report a new method to prepare Fe_3O_4—Ag composite nanoparticles by *in situ* reduction of Ag on a magnetic core of Fe_3O_4, focusing the attention on the effect of process parameters (synthesis media and functionalization steps) on the nanoparticles nucleation and morphology. In particular, Gallic Acid (GA) has been used for the first time, on the basis of authors knowledge, as *in situ* reducing agent for Ag nanoparticles directly on Fe_3O_4 NPs' surface. GA has been chosen for its above mentioned double action, as well as for its intrinsic anti-inflammatory and anti-tumor action, and for its potential sustainability, due to the possibility to be extracted from vegetal wastes coming from the food production chains [31]. The obtained composite NPs, due to both the magnetic properties of Fe_3O_4 and the optical/antibacterial properties

of Ag NPs, can be a useful tool for targeting bacterial infection as well as for treating tumor and associated complications.

2. Experimental

Each experimental step is described in the following paragraphs. All reactants were purchased from Sigma Aldrich®/ Merck.

2.1 Synthesis of CA stabilized MNPs

The synthesis of Fe_3O_4 NPs (Magnetite-based - M NPs) was carried out by co-precipitation [32-34]. As reported also in [10, 11], M NPs were synthesized by mixing aqueous solution of Fe^{2+} and Fe^{3+} salts in alkaline conditions for ammonium hydroxide NH_4OH (Merck, 25% aqueous solution) [5]. Two solutions 0.1 M of ferrous chloride $FeCl_2 \cdot 4\ H_2O$ and ferric chloride $FeCl_3 \cdot 6H_2O$ (Sigma Aldrich, > 99%) were prepared separately by dissolving the required quantities of $FeCl_2 \cdot 4H_2O$ and $FeCl_3 \cdot 6H_2O$ in 100 ml of bi-distilled water, magnetically stirred in two distinct beakers. The pH was around 3 for the ferrous chloride solution, and around 2 for the ferric chloride solution. After the complete dissolution of the salts, 50 ml of 0.1M $FeCl_3 \cdot 6H_2O$ and 37.5 ml of the 0.1M $FeCl_2 \cdot 4H_2O$ were mixed in a beaker, reaching a pH value around 1.7.

The pH was then adjusted to about 10 by adding NH_4OH dropwise to the iron salts solution, under continuous mechanical stirring: the mixture turned to black, due to the formation of a suspension of iron oxide NPs (M NPs).

The as obtained suspension was then sonicated for 20 minutes and washed in bi-distilled water, using a magnet to induce sedimentation. The as obtained M NPs were finally re-suspended in 100 ml of bi-distilled water reaching a pH between 7-8.

Aiming to improve the MNPs suspension stability, the synthesis was followed by the M NPs stabilization with Citric Acid (CA) [32, 33]. 120 ml of a 0.05 M of CA (Sigma Aldrich, > 99.5%) solution were added to the M NPs, previously separated by sedimentation, adjusting the pH to a value of 5.2 by adding dropwise a concentrated NH_4OH solution. The new suspension was then heated to 80 °C and stirred (150 rpm) for 90 minutes. The duration of the heating step was optimized in order to promote the CA adsorption on the M NPs while minimizing the magnetite decomposition to maghemite. Finally, the CA-capped MNPs were rinsed by means of an ultrafiltration device (Solvent Resistant Stirred Cells - Merck Millipore)(4 steps in 50 ml of bi-distilled water at pH = 10.2) and suspended in 120 ml of bi-distilled water, adjusting the pH of the final water suspension to 10.2 with diluted ammonia.

2.2 Silica coating on MNPs

A part of CA-capped MNPs was coated with a silica shell following the Stöber method [34] by suspending them in a mixture of Tetraethyl orthosilicate (TEOS) as silica precursor, ethanol and water (ethanol:water volume ratio of 4:1), under stirring in orbital shaker at 37 °C and 150 rpm for 3 hours. Approximately 0.002 ml of TEOS for each mg of magnetic nanoparticles was used. Then, the obtained MS NPs were double-washed with bi-distilled water using an ultrafiltration device and re-dispersed in water.

2.3 Functionalization with aminopropyltriethoxysilane (APTES)

To enhance the interaction between Ag NPs and magnetic NPs, terminal $-NH_2$ groups were introduced on the surface of both M NPs (route A) and MS NPs (route B) by means of functionalization with APTES (> 98%, Merck).

The functionalization with APTES on the M NPs was performed including a final step of washing and re-suspension in two different media (ethylic alcohol or water) in order to verify the role of the medium on GA grafting and, in turn, on the nucleation of Ag NPs. MS NPs were resuspended only in water.

For this step, 3 ml of each magnetic NPs suspension were diluted in 50 ml of absolute ethanol (anhydrous, >99.9%, Carlo Erba Reagents) and sonicated for 3 minutes. 10 µl of APTES were then added to the resulting colloidal suspensions. The obtained suspensions were then heated at 80 °C under mechanical stirring for three hours. The stirring time has been prolonged respect to the conventional synthesis reported in literature, to enhance the APTES grafting and assure a uniform presence of terminal amine group on the magnetic nanoparticles surface, as reported in previous works [10, 11, 35]. Subsequently, the mixtures were cooled at room temperature, the nanoparticles were magnetically separated and centrifuged (7500 rpm /20 minutes) for three times, washed in distilled water and re-suspended in water or ethanol (M NPs) or only in water (MS NPs) up to a volume of 50 ml. To induce positive charge at the surface of the APTES-coated nanoparticles, a diluted HNO_3 solution (0.05 ml of 6 M HNO_3 with 20 ml of water) was added drop by drop until reaching a pH value ≈ 5-6, and stirred for 10 minutes.

2.4 Functionalization with GA

Gallic acid (GA) was added to both ethanol and water-based M NPs suspensions using two different NPs/GA weight ratio (10:3 and 10:1) [37] and to water-based MS NPs suspension using a NPs/GA weight ratio of 10:1. The mixtures were stirred for 18 h at 80 °C, at the end of the treatment the NPs dispersed in ethanol were washed and centrifuged

three times with ethanol and re-suspended in ethanol; the same procedure was adopted for NPs dispersed in water, using bi-distilled water as washing and dispersion medium. Figure 1 resumes the steps of the functionalization process.

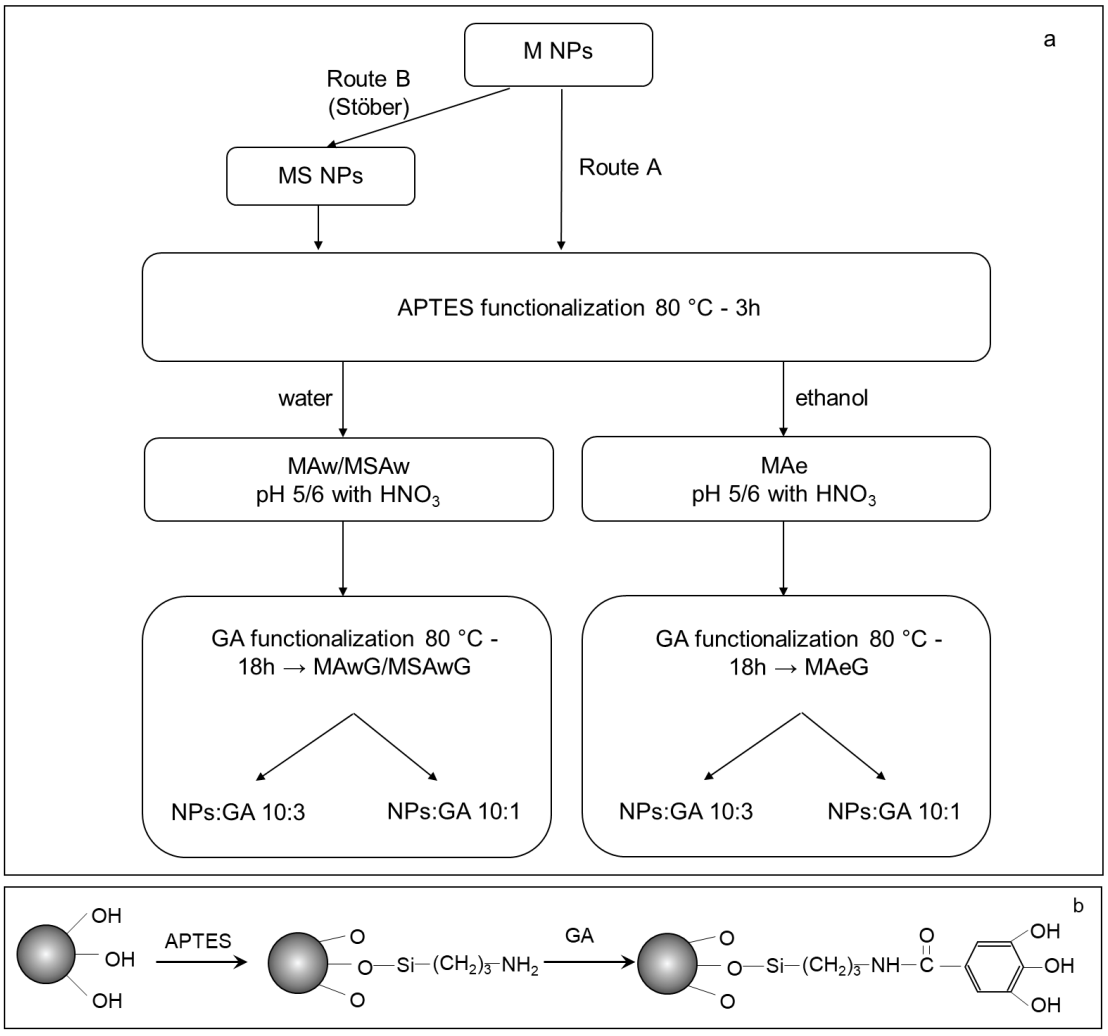

Figure 1: functionalization process (a) and scheme (b) of MAwG and MAeG synthesis.

2.5 Synthesis of Fe_3O_4—Ag composite nanoparticles

The reduction of Ag NPs was performed both for ethanol and water dispersed M NPs and MS NPs, using a $AgNO_3$/GA weight ratio of 1.7. $AgNO_3$ was dissolved in water and mixed with the NPs suspension at 37 °C for 15 minutes at 150 rpm; the pH of the mixture was adjusted to about 11 using NH_4OH. At the end of the synthesis the mixture was

179 washed with bi-distilled water, NPs were magnetically separated and re-dispersed in bi-
180 distilled water for further analysis.

181 Table 1 reports the acronyms of the obtained NPs and resume their synthesis steps.

	Magnetite	**Silica shell**	**Synthesis in water (w) or ethanol (e)**	**APTES**	**Gallic acid (GA)**	**Silver**
M	✓					
MAw	✓		w	✓		
MAe	✓		e	✓		
MAwG	✓		w	✓	✓	
MAeG	✓		e	✓	✓	
MAwGAg	✓		w	✓	✓	✓
MAeGAg	✓		e	✓	✓	✓
MS	✓	✓				
MSAw	✓	✓	w	✓		
MSAwG	✓	✓	w	✓	✓	
MSAwGAg	✓	✓	w	✓	✓	✓

182

183 **Table 1**: acronyms and resume of NPs synthesis steps.

184

185 **2.6 Characterization**

186 The structural characterization of M NPs was carried out by means of wide-angle (2θ
187 within 10-70°) X-ray diffraction analysis (XRD – X'Pert Philips diffractometer) using
188 the Bragg Brentano camera geometry and CuKa incident radiation. The identification of

crystalline phases was performed by using X'Pert HighScore program equipped with PCPDFWIN database.

To evaluate the effective functionalization with APTES and GA, all NPs before the *in situ* reduction of silver were analyzed by means of Fourier-transform infrared spectroscopy (FTIR Tensor 27, Bruker Optics S.p.A, Ettlingen, Germany) from 4500 to 300 cm^{-1} and with 2 cm^{-1} resolution. OPUS software (v. 6.5, Bruker S.p.A) was used for instrumental control and spectral acquisition.

In order to investigate the NPs functionalization after each synthesis step, the formation of Ag NPs and their dimension and distribution, all nanoparticles were characterized in terms of morphology and composition by means of FESEM (Field-Emission Scanning Electron Microscope - SUPRATM 40, Zeiss, Germany) and STEM (Scanning Transmission Electron Microscopy - Merlin Gemini Zeiss, Germany), equipped with Energy Dispersive Spectroscopy (EDS). For STEM observation a drop of each NPs suspension was placed on a copper grid with carbon film (SPI Supplies® Brand Lacey Carbon Coated 200 Mesh Copper Grids – JEOL S.p.A.). STEM analyses were carried out using different detectors and signals (secondary and backscattered electrons, the Bright Field - BF and Dark Field – DF) in order to better distinguish the metallic NPs.

3. Results

3.1 Route A

Morphological (FESEM) and phase (XRD) analyses of M NPs (Figure 2) revealed the presence of NPs with spherical morphology and a diameter of about 5-20 nm. The XRD pattern reports the presence of only magnetite/maghemite phase, in accordance with the synthesis performed in air.

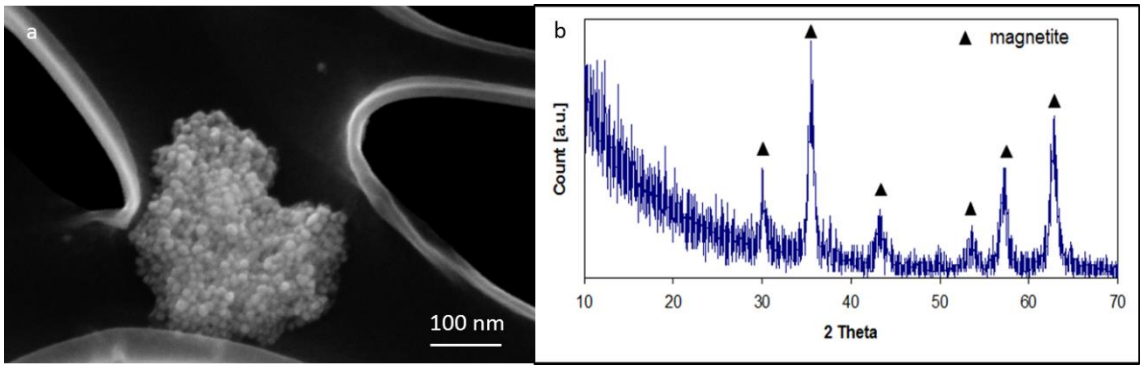

Figure 2: CA stabilized M NPs: a) morphological evaluation (FESEM), b) XRD analysis

Table 2 reports the peaks and bands identified by FTIR analysis of M NPs (stabilized with CA), MAw, MAwG, MAe and MAeG. Figure 3 shows as example the curves obtained for M, MAw and MAwG NPs/GA 10:3. As it can be noticed, M NPs spectrum shows the presence of Fe-O bond between 500-600 cm^{-1} typical of iron-oxide NPs [38], the asymmetric stretching of C-O from the COOH group of CA at 1310 cm^{-1}, the large peak between 1400 cm^{-1} and 1660 cm^{-1} can be assigned both to COO-Fe bonding (in literature 1431 cm^{-1}) and to the shift of peak characteristic of symmetric vibration of C=O due to the CA interaction with magnetite; moreover a band at about 1700 cm^{-1}, relative to the C=O stretching vibration from the free COOH group of CA, is still visible. In the curve a band between 2600-2950 cm^{-1}ascribable to CH_2 stretching and a barely resolvable band at about 3300 cm^{-1} due to OH stretching are also observable [38-40]. The MAw NPs spectrum shows a shoulder at 850-950 cm^{-1} ascribable to the stretch of Si-OH symmetric vibration or Si-O-Fe bond, and two bands around 960 and1000-1150 cm^{-1} belonging to the stretching of Si-O and Si–O–Si groups. The peaks at about 1330 and 1620 cm^{-1} relative to C-N and NH stretching vibrations respectively, the band between 2920-2850 cm^{-1} ascribable to the stretching and vibration of C-H and the bands at 3445 and 1640 cm^{-}

^{1}, attributable to the N–H stretching vibration and NH_2 bending mode of free NH_2 groups [41-43], are hardly attributable due to the overlapping with CA peaks.

The functionalization with GA introduces three peaks between 1600-1200 cm^{-1} ascribable to the C=C bond, a small peak at about 1700 cm^{-1} relative to the C=O stretch of carboxylic group and a band centered at about 3400 cm^{-1} relative to OH groups of GA [44, 45].

FTIR spectra of M, MAe and MAeG (obtained peaks reported in table 2) evidence a band between 400 and 500 cm^{-1} ascribable to Fe-O bond and the peak at 1310 cm^{-1} due to the asymmetric stretching of -CO from the COOH group, the peak probably due to both the COO-Fe bond and to the C=O of COOH group that interact with magnetite NPs, the C=O vibration from the free COOH group of CA at about 1700 cm^{-1} [38, 40]. The functionalization with APTES is confirmed by the presence of a shoulder at about 970 cm^{-1} ascribable to Si-O stretching, a peak at about 1100 cm^{-1} due to the Si-O-Si stretching and the shoulder at about 2870 cm^{-1} is related to the stretching vibration C-H. Even if after the synthesis the NPs were washed, some characteristic peaks of ethanol (not reported in table 2) can be observed in the spectrum of MAe at about 1260-1000 cm^{-1} ascribable to the stretching of C-O and between 3400-3300 cm^{-1} related to the OH stretching. Both the influence of the residual ethanol and the CA disturb the identification of the peaks relative to the C-N stretching vibration and, the free NH stretching vibration [41-43]. The spectrum of MAeG shows three peaks between 1600-1200 cm^{-1} ascribable to the C=C bond and a very small peak at about 1700 cm^{-1} relative to the C=O stretch of carboxylic group, the band at about 3400 cm^{-1} relative to OH groups of GA in this case is poor visible [44, 45].

Assignment	**Position (cm^{-1})**	**Remarks**

Fe-O	500-600	Typical of iron-oxide NPs (M, MAw, MAwG, MAe, MAeG)
Si-OH, Si-O-Fe	850-950	A shoulder related to the stretch of Si-OH symmetric vibration or Si-O-Fe bond (MS, MSAw, MSAwG)
Si-O	960-970	A band due to the Si-O stretching (MAw, MAwG, MAe, MAeG)
Si–O–Si	1000-1150	A band belonging to the stretching of Si–O–Si groups (MAw, MAwG, MAe, MAeG)
C=C	1200-1600	A peak ascribable to the C=C bond (MAeG, MAeG)
C-O	1310	The asymmetric stretching of C-O from the COOH group of CA (M, MAw, MAwG, MAe, MAeG)
C-N	1330	The peak related to C-N stretching vibration (MAw, MAwG, MAe, MAeG)
COO-Fe, C=O	1400-1600	The large peak can be assigned both to COO-Fe bonding (in literature 1431 cm^{-1}) and to the shift of peak characteristic of symmetric vibration of C=O due to the CA interaction with magnetite (M, MAw, MAwG, MAe, MAeG)
NH	1620	A broad band at 1628 cm−1 can be ascribed to the N–H stretching vibration (MAw, MAe)

NH_2	1640	The band attributable to NH_2 bending mode of free NH_2 groups (MAw, MAe)
C=O	1700	Stretching vibration from the free COOH group of CA (M, MAw, MAwG, MAe, MAeG)
C=O	1700	A small peak related to the C=O stretch of carboxylic group (MAwG, MAeG)
CH_2	2600-2950	A band ascribable to CH_2 stretching (M, MAw, MAwG, MAe, MAeG)
C-H	2850-2920	The band ascribable to the stretching and vibration of C-H (MAw, MAeG, MAe, MAeG)
OH	3300-3400	A band related to OH groups (M, MAw, MAwG, MAe, MAeG)
N-H	3445	The bands attributable to the N–H stretching vibration (MAw, MAwG, MAe, MAeG)

Table 2: List of the main peaks detected in the FTIR spectra of M, MAw, MAwG, MAe, MAeG, MS, MSAw and MSAwG NPs.

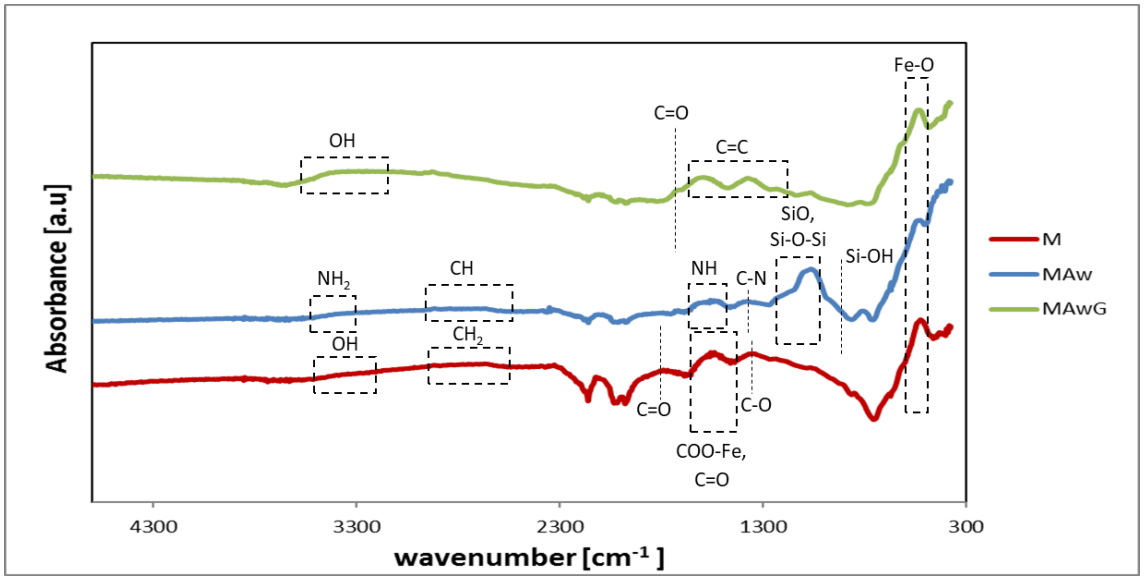

Figure 3: FTIR spectra of M, MAw and MAwG (NPs/GA 10:3) NPs.

The morphological and compositional analysis of MAeG (Figure 4a-c) shows the presence of spherical particles with a diameter between 5-20 nm. The EDS analysis (Figure 4c, MAeG with NPs/GA 10:1 as example) shows the Si peak ascribable to APTES functionalization. Analogously, the morphological analysis of MAwG (Figure 4d-e) reveals the presence of NPs with pseudo-spherical morphology and a diameter of about 5-20 nm. Also in this case the compositional analysis performed on MAwG with NPs/GA 10:1 (Figure 4f) evidences the peak of Si, due to the APTES functionalization.

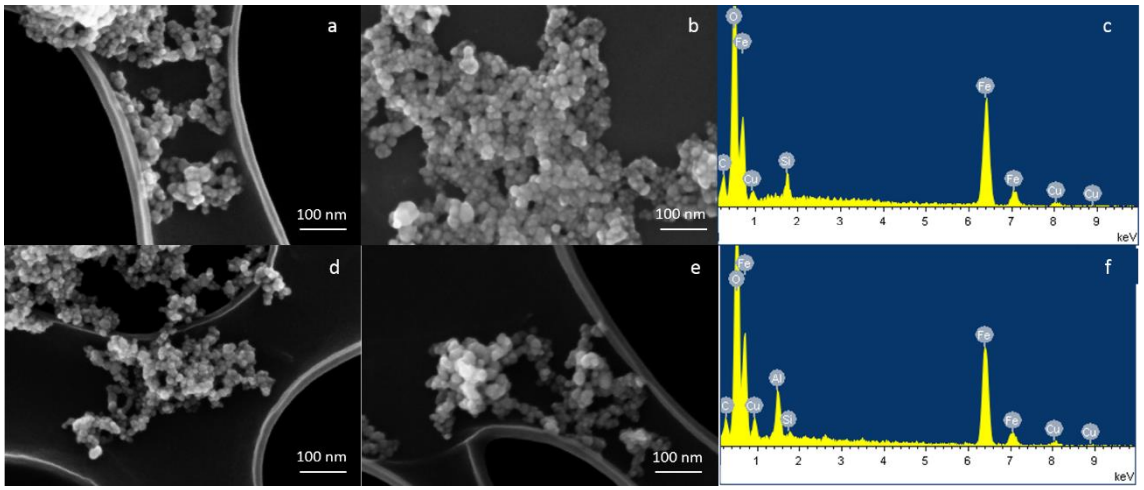

Figure 4: FESEM-EDS analysis of a) MAeG 10:1, b) MAeG 10:3, c) MAeG 10:1, d) MAwG 10:1, e) MAwG 10:3, f) MAwG 10:1.

The STEM-EDS analysis of MAeGAg is reported in figure 5; as it can be observed MAeGAg performed using NPs/GA ratio 10:1 show the presence of Ag nanometric particles (< 50 nm) agglomerated with magnetite nanoparticles, evidenced with arrows in figure 5a together with big silver particles (100-150 nm) with different shape (Figure 5b). The EDS of area (Figure 5c) shows the peak of Ag, together with elements characteristic of MAeG (Fe, Si and O) and elements acribable to sample holder (Cu, Al, C).

MAeGAg performed using NPs/GA ratio 10:3 show the presence of very small Ag NPs (< 10 nm), which forms a nanoflower structure with magnetic NPs (Figure 5d, evidenced by arrows and schematized in the inset). However, also in this case, in some area of the sample big silver crystals were observed (Figure 5f and e) as confirmed by the EDS analysis (Figure 5f).

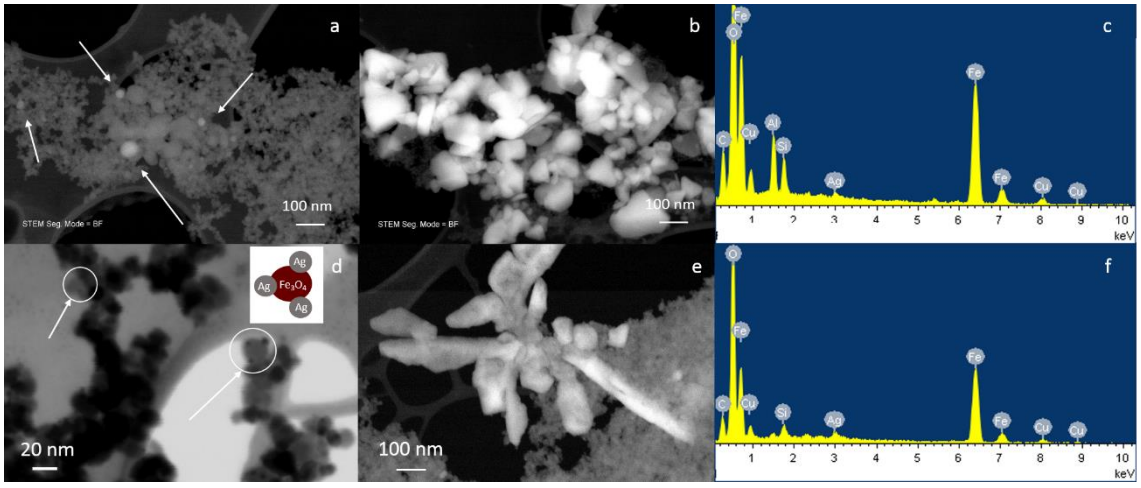

Figure 5: FESEM-EDS analysis of MAeGAg 10:1 (a-c) and MAeGAg 10:3 (d-f).

Figure 6 shows the STEM-EDS analysis of MAwGAg; in this case only Ag nanoparticles with dimension comparable with magnetite NPs were observed both for NPs/GA ratio 10:1 (Figure 6a and b) and 10:3 (Figure 6d and e). Thus, in both NPs/GA ratio conditions, the synthesis in water allowed to obtain nanodumbbell structures with magnetite NPs connected with Ag NPs (Figure 6b and 6e). EDS analysis (Figure 6c and f) shows the Ag peak in addition to magnetic NPs peaks. As far as concerned the stability of composite NPs, their visual inspection suggests that they form a fairly stable suspension. Future test will be carried out to experimentally evaluate the stability of the nanostructures over time.

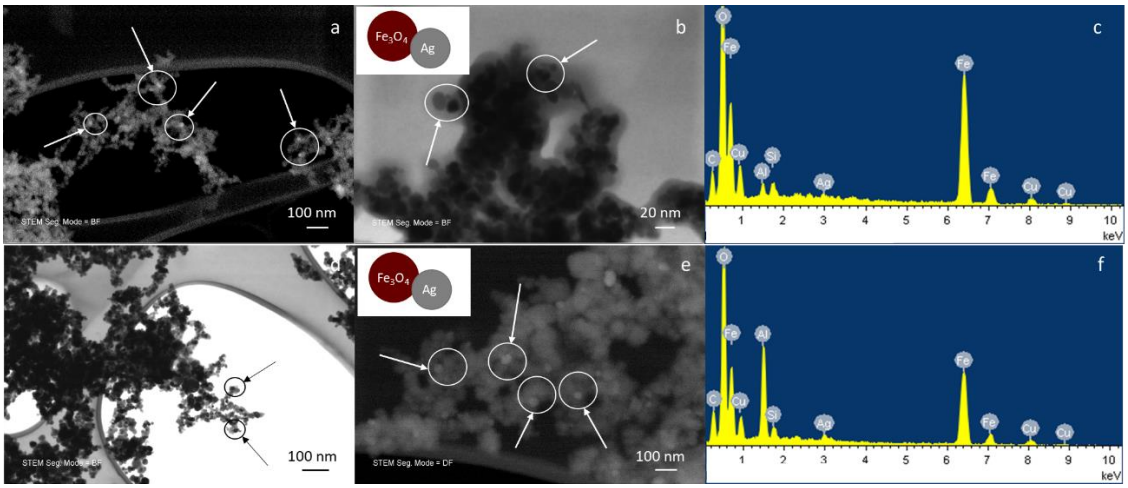

Figure 6: STEM-EDS analysis of MAwGAg 10:1 (a-c) and MAwGAg 10:3 (d-f).

3.2 Route B

The peaks obtained by means of FTIR analysis of MS, MSAw and MSAwG nanoparticles are reported in table 2. MS NPs evidence both the peak ascribable to Fe-O bond at about 500-600 cm^{-1} and the peak characteristic of silica shell: at 780 cm^{-1} the stretch of Si-OH, the broad band at about 850-990 cm^{-1} can be attributed to the Si-O symmetric vibration or to the Si-O-Fe bond and the peak at 1060 cm^{-1} the stretch of Si-O-Si [46, 47]. The

spectrum of MSAw shows an increase of the intensity of the peak related to Si-O-Si bond attributable to the APTES functionalization, together with the peak of Fe-O bond. The spectrum of MSAwG shows the peeks between 1600-1200 cm^{-1} ascribable to the C=C bond, the peak at about 1700 cm^{-1} relative to the C=O stretch of carboxylic group, the band at about 3400 cm^{-1} relative to OH groups of GA [44, 45].

The morphological analysis of MSAwG (Figure 7a) evidences the presence of pseudo-spherical nanoparticles in the range 10-20 nm. The EDS spectrum (Figure 7b) shows a very intense peak of Si ascribable to the silica shell, together with Fe and O peak; C peak is due to the grid.

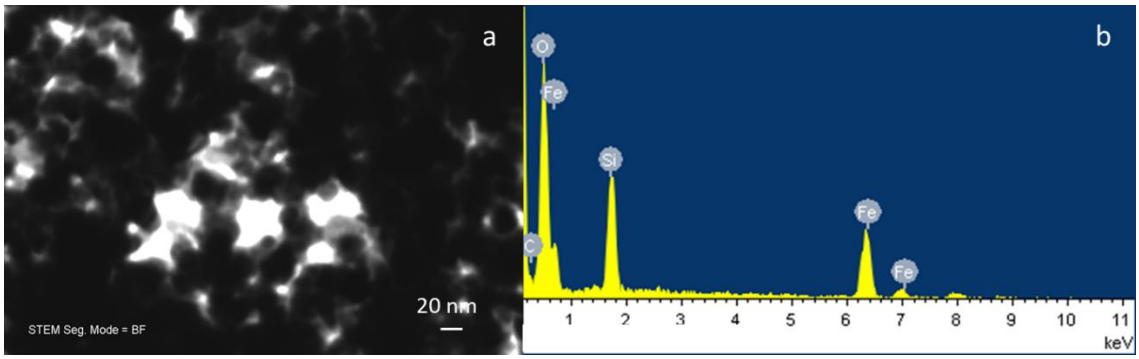

Figure 7: STEM image and EDS analysis of MSAwG.

The STEM analysis of MSAwGAg (Figure 8a) shows the formation of Ag NPs of ≤ 20 nm not well dispersed among magnetic NPs, but aggregated in some area (schematic representation in Figure 8a); compositional analysis of an area (Figure 8b) shows the effective presence of the Ag peak.

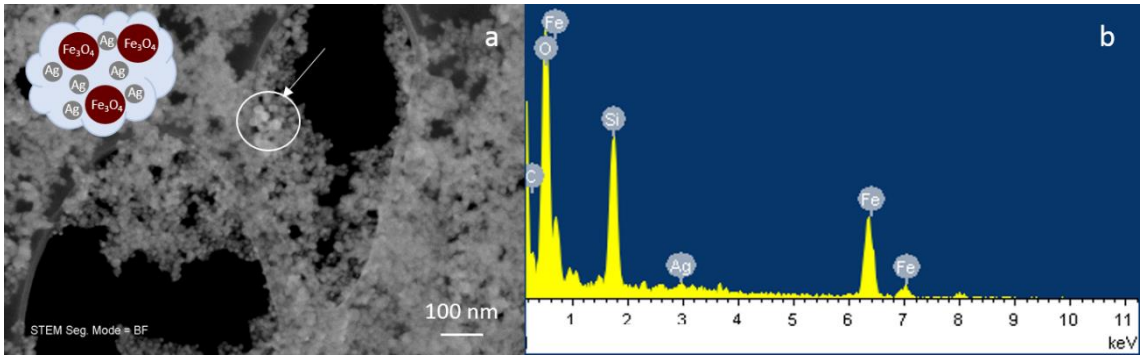

Figure 8: STEM-EDS analysis of MSAwGAg obtained using a NPs/GA ratio of 10:1.

4. Discussion

Aiming to improve the MNPs suspension stability, useful also for further functionalization steps, the prevention of their aggregation is a crucial aspect. In fact, the stability of MNPs in water is not optimal, due to anisotropic dipolar attraction [48] that could limit the nucleation of the metal nanoparticles on their surface [49]. For this purpose, CA was added to the MNPs suspension as stabilizing agent, promoting electrostatic repulsion, as reported also by several authors [48, 50, 51].

Concerning the functionalization with APTES and GA, no significant differences were noticed by FTIR analysis, although in the synthesis performed in ethanol it was difficult to identify some characteristic groups due to probable traces of residual ethanol.

The morphological and compositional analysis of samples synthesized in water evidenced the nucleation of smaller Ag nanoparticles by using a NPs/GA ratio of 10:3. We supposed that the higher amount of GA used in this synthesis introduced more nucleation sites allowing the formation of a lot of very small Ag NPs. In any case, even in this synthesis some larger Ag crystals, with a multibranched morphology, were noticed. These crystaks could have been originated due to the seeding role of the nanoflwoers-like structures, as

reported for ternary heterostructures by H. Zeng and S. Sun [52], further enhanched by the excess of reducing agent in the synthesis environment.

The sintheses performed in water revealed the formation of small Ag nanoparticles both using a NPs/GA ratio of 110:1 and 10:3. This result could be explained considering that, as reported by [52], the partial exposure of Fe(II) on the nanoparticles to aqueous phase could act as self-catalytic center for the reduction of Ag^{+} ions to Ag° nanoparticles, leading to the heterodimer morphology.

In summary, the synsthesis in water allows to obtain more homogenoeus heterodimer nanostructures, while the ethanol-based synthesis seems to have some critycal aspects in the control of the dimension and structure of silver NPs. Moreover, in the syntesis in water, the different ratio between NPs and GA amount seems to not significantly influence the amount and dimension of Ag NPs. For this reason, the route B was perfomed only in water using a NPs/GA ratio of 10:1.

The NPs coating with a shell of silica seems to not improve the NPs functionalization and most of all the *in situ* reduction of Ag NPs; in this case some small aggregates of Ag NPs, not uniformely distributed were observed. As reported in other studies [47, 53], the structure of nanocomposites is significantly influenced by charges, reactive groups or functional moieties on the nanoparticles surface. The role of silica layer in the precipitation of the above mentioned aggregates can be explained considering that bi-component hybrid nanoparticles are generally obtained by sequential nucleation and growth of the second component on a preformed seed of the first one [52]. The successful synthesis of heterodimers strongly depends on the ability of suppressing the formation of dispersed NPs of the second component (homogeneous nucleation) and promote their seed-mediated heterogeneous nucleation on the first component NPs. This could be

365 achieved if the lattice spacing between the two components is well-matched to ensure
366 epitaxial growth of the second component on the first one, which often participate to the
367 reaction as catalyst, lowering the activating energy for heterogeneous nucleation. The
368 obtained results demonstrated that the silica shell seems to not positively influence the
369 decoration of MS NPs, probably due to its shield effect on the heterogeneous nucleation
370 of Ag NPs, while promoting their homogeneous nucleation in the synthesis medium and
371 their aggregated with the MS NPs, due to electrostatic interactions. Thus, the silver *in situ*
372 reduction by GA and the heterogeneous nucleation are promoted when magnetic NPs are
373 not coated by the silica shell; these two mechanisms are synergistic and lead to a better
374 decoration of magnetite NPs. In particular, if magnetic NPs are not coated by silica, they
375 are able to expose Fe(II) supporting the heterogeneous nucleation of Ag NPs, in addition
376 to the *in situ* reduction due to GA.
377
378 **5. Conclusions**
379 A novel method to prepare composite nanoparticles Fe_3O_4—Ag, by *in situ* reduction of
380 Ag on a magnetic core of Fe_3O_4 was developed. The synthesis allowed at first to prepare
381 Fe_3O_4 NPs stabilized by CA with spherical shape and size in the range 5 – 20 nm. The
382 obtained CA capped Fe_3O_4 NPs were successfully functionalized with APTES to graft
383 GA, as reducing agent for Ag NPs, in different media and with different NP/GA ratios.
384 Depending on the investigated synthesis conditions, different morphologies were
385 obtained, from polydispersed aggregates to nanoflower-like and nanodumbbell
386 nanocomposites. The best results were obtained in aqueous media, with NPs/GA ratio of
387 10:1, producing Fe_3O_4—Ag well defined nanodumbbells of about 20 nm size.

A further sol-gel coating of the CA-capped Fe_3O_4 NPs with a silica shell, functionalized with APTES and GA in aqueous medium, was performed to assess its influence on the nucleation of Ag NPs. In the presence of the silica coating, Ag NPs with size < 20 nm nucleated as polydispersed aggregated among Fe_3O_4 NPs, evidencing that the silica shell is not a key issue to optimize the morphology of Ag NPs nucleated on the magnetic core. Further optimizations of synthesis parameters (such as time and reagent ratio) are still necessary to improve the size and distribution of Ag NPs on Fe_3O_4 NPs. The electromagnetic and optical characterizations are still in progress, as well as the evaluation of suspensions stability.

Summary Points

1. Development of a novel method to prepare composite nanoparticles Fe_3O_4—Ag, by in situ reduction of Ag on a magnetic core
2. Use of gallic acid, a green anti-inflammatory and anti-tumor phenolic compound, as *in situ* reducing agent for Ag NPs
3. Evaluation of different synthesis media and functionalization steps
4. Estimation of different gallic acid/NPs rations
5. Successfully functionalization of magnetic NPs with APTES and grafting with GA, both in water and ethanol
6. Polydispersed aggregates, nanoflower-like and nanodumbbell nanocomposites were obtained according to the synthesis conditions
7. Well-defined Fe_3O_4—Ag nanodumbbells (about 20 nm) were obtained using aqueous media, a NPs/GA ratio of 10:1

8. The presence of a silica coating was not found to be useful to optimize the morphology of Ag NPs nucleated on the magnetic core

Acknowledgements

Elisa Bertone, previously working as research fellow at DISAT, is kindly acknowledged for FTIR measurements.

References

[1] Rahman MM, Nanomaterials, 356. ISBN: 978-953-307-913-4, (2011). DOI: 10.5772/1371

[2] Wu W, Wu Z, Yu T, Jiang C, Kim WS. Recent progress on magnetic iron oxide nanoparticles: synthesis, surface functional strategies and biomedical applications. *Sci. Technol. Adv. Mater.* 16, 023501(2015). DOI: 10.1088/1468-6996/16/2/023501.

[3] Tartaj P, Morales MP, Veintemillas-Verdaguer S, Gonzalez-Carreno T, Serna CJ. The preparation of magnetic nanoparticles for applications in biomedicine *J. Phys. D. Appl. Phys*. 36, 182-197 (2003). DOI: 10.1088/0022-3727/36/13/202

[4] Veiseh O, Gunn J, Zhang M, Design and fabrication of magnetic nanoparticles for targeted drug delivery and imaging. *Adv. Drug. Deliv. Rev.* 62(3), 284–304 (2010). doi: 10.1016/j.addr.2009.11.002

[5] Li Z, Kawashita M, Araki N, Mitsumori M, Hiraoka M, Do M. Magnetite nanoparticles with high heating efficiencies for application in the hyperthermia of cancer. *Mater. Sci. Eng. C.* 30, 990–996 (2010). Doi:10.1016/j.msec.2010.04.016

[6] Prucek R, Kilianová TJ, Panáček M et al.The targeted antibacterial and antifungal properties of magnetic nanocomposite of iron oxide and silver nanoparticles. *Biomaterials* 32, 4704-4713 (2011). doi: 10.1016/j.biomaterials.2011.03.039

[7] Kluchova K, Zboril R, Tucek J, et al. Superparamagnetic maghemite nanoparticles from solid-state synthesis - their functionalization towards per oral MRI contrast agent and magnetic carrier for trypsin immobilization. *Biomaterials* 30, 2855 (2009). doi: 10.1016/j.biomaterials.2009.02.023

[8] Corr SA, Rakovich YP, Gun'ko YK. Multifunctional magnetic-fluorescentnanocomposites for biomedical applications. *Nanoscale Res. Lett.* 3, 87 (2008). doi: 10.1007/s11671-008-9122-8

[9] Srivastava P, Sharma PK, Muheem A, Warsi MH. Magnetic Nanoparticles: A Review on Stratagems of Fabrication and its Biomedical Applications. *Recent Patents on Drug Delivery & Formulation*, 11, 101-113 (2017). doi.:10.2174/1872211311666170328150747

[10] Miola M, Ferraris S, Pirani F. et al. Reductant-free synthesis of magnetoplasmonic iron oxide-gold nanoparticles *Ceramics International* 43, 15258–15265 (2017). DOI: 10.1016/j.ceramint.2017.08.063

[11] Multari C, Miola M, Laviano F, et al. Magnetoplasmonic nanoparticles for photothermal therapy. *Nanotechnology* 30, 255705 (9pp) (2019). doi:10.1088/1361-6528/ab08f7

[12] Mohan YM, Lee K, Premkumar T, Geckeler KE. Hydrogel networks as nano-reactors: a novel approach to silver nanoparticles for antibacterial applications. *Polymer* 48, 158 (2007). Doi:10.1016/j.polymer.2006.10.045

[13] Wang AQ, Liu JH, Lin SD, Lin TS, Mou CY. A novel efficient Au-Ag alloy catalyst system: preparation, activity, and characterization. *J Catal* 233, 186. (2005) doi.org/10.1016/j.jcat.2005.04.028

[14] Lee D, Cohen RE, Rubner MF. Antibacterial properties of Ag nanoparticle loaded multilayers and formation of magnetically directed antibacterial microparticles. *Langmuir* 21, 9651 (2005). Doi:10.1021/la0513306

[15] Zhang XF, Liu ZG, Shen W, Gurunathan S. Silver Nanoparticles: Synthesis, Characterization, Properties, Applications, and Therapeutic Approaches. *Int. J. Mol. Sci.* 17(9) 1534 (2016). doi: 10.3390/ijms17091534

[16]Markova Z, Šiskova KM, J. Filip et al. Air Stable Magnetic Bimetallic Fe−Ag Nanoparticles for Advanced Antimicrobial Treatment and Phosphorus Removal. *Environ. Sci. Technol.* 47, 5285−5293 (2013). Doi:10.1021/es304693g

[17] Lee HJ, Yeo SY, Jeong SH. Antibacterial effect of nanosized silver colloidal solution on textile fabrics. *J. Mater. Sci.* 38, 2199 (2003). Doi:10.1023/A:1023736416361

[18] Pal S, Tak YK, Song JM. Does the antimicrobial activity of silver nanoparticles depend on the shape of the nanoparticle? a study of the gram-negative bacterium Escherichia coli. *Appl. Environ. Microbiol.* 73, 1712. (2007) DOI: 10.1128/AEM.02218-06

[19] Wu YX, Liang P, Dong Q, et al.Design of a silver nanoparticle for sensitive surface enhanced Raman spectroscopy detection of carmine dye. *Food Chemistry* 237, 974-980 (2017). Doi: 10.1016/j.foodchem.2017.06.057

[20] Zhang H, Chen G, Yu B, Cong H. Emerging advanced nanomaterials for Cancer photothermal therapy. *Rev.Adv. Mater. Sci.* 53, 131-146 (2018). DOI: 10.1515/rams-2018-0010

[21] Ching G, Jiang J, Ying JY, Ji W. Fe_3O_4-Ag nanocomposites for optical limiting: broad temporal response and low threshold. *Opt Express*18, 6183 (2010). DOI: 10.1364/OE.18.006183

[22] Laurent S, Forge D, Port M, et al. Magnetic Iron Oxide Nanoparticles: Synthesis, Stabilization, Vectorization, Physicochemical Characterizations, and Biological Applications. *Chem. Rev.*, 108(6), 2064–2110 (2008). DOI: 10.1021/cr068445e

[23] Kharisov BI, Rasika Dias HV, Kharissova OV, Vázquez A, Peña Y Gómez I. Solubilization, dispersion and stabilization of magnetic nanoparticles in water and non-aqueous solvents: recent trends. *RSC Adv* ,4, 45354-45381 (2014). DOI: 10.1039/C4RA06902A

[24] Stafford S, Serrano Garcia R, Gun'ko YK. Multimodal Magnetic-Plasmonic Nanoparticles for Biomedical Applications. *Appl. Sci.* 8, 97 (2018). doi:10.3390/app8010097

[25] Abbas M, Ramulu Torati S, Kim C. A novel approach for the synthesis of ultrathin silica-coated iron oxide nanocubes decorated with silver nanodots (Fe_3O_4/SiO_2/Ag) and their superior catalytic reduction of 4-nitroaniline. *Nanoscale*, 7, 12192-12204 (2015). DOI: 10.1039/C5NR02680F

[26] Lee B, Koo S. Silver reduction on the surface of magnetite nanoparticles using a coupling agent. *J.Ind. and Eng. Chem.*18(3), 1191–1195(2012). Doi: 10.1016/j.jiec.2012.01.009

501 [27] Ballesteros CAS, Cancino J, Marangoni VS, Zucolotto V. Nanostructured Fe_3O_4
502 satellite gold nanoparticles to improve biomolecular detection. *Sensors and Actuators B*
503 198, 377–383 (2014). doi.: 10.1016/j.snb.2014.03.079
504 [28] Fantechi E, Castillo PM, Conca E, Cugia F, Sangregorio C, Casula MF, Assessing
505 the hyperthermic properties of magnetic heterostructures: The case of gold–iron oxide
506 composites. *Interface Focus* 6, 20160058 (2016). doi: 10.1098/rsfs.2016.0058
507 [29] Ivashchenko O, Gapinski J, Pepli´nska B. et al.Self-organizing silver and ultrasmall
508 iron oxide nanoparticles prepared with ginger rhizome extract: Characterization,
509 biomedical potential and microstructure analysis of hydrocolloids. *Mater. Design* 133,
510 307–324 (2017). doi.: 10.1016/j.matdes.2017.08.001
511 [30] Amala Jayanthi S, Manovah David T, Jayashainy J, Muthu Gnana D, Nathan T,
512 Sagayaraj P. A convenient two-step bottom-up approach for developing Au/Fe_3O_4
513 nanocomposites with useful optical and magnetic properties. *J. Alloys and Compounds*
514 606, 254–226 (2014). DOI: 10.1016/j.jallcom.2014.03.186
515 [31] Ferraris S, Miola M, Cochis A. et al.In situ reduction of antibacterial silver ions to
516 metallic silver nanoparticles on bioactive glasses functionalized with Polyphenols. *Appl.*
517 *Surf.Sci.* 396, 461–470 (2017). doi.: 10.1016/j.apsusc.2016.10.177
518 [32] Borroni E, Miola M, Ferraris S. et al.Tumor targeting by lentiviral vectors
519 combined with magnetic nanoparticles in mice. *Acta Biomaterialia* 59, 303–316 (2017).
520 doi: 10.1016/j.actbio.2017.07.007.
521 [33] Multari C, Miola M, Ferraris S. et al.Synthesis and characterization of silica-coated
522 superparamagnetic iron oxide nanoparticles and interaction with pancreatic cancer cells.
523 *Int J Appl Ceram Technol*. 15, 947–960 (2018). Doi: 10.1111/ijac.12897

524 [34] Muzio G, Miola M, Ferraris S, et al.A. Follenzi. Innovative superparamagnetic
525 iron-oxide nanoparticles coated with silica and conjugated with linoleic acid: Effect on
526 tumor cell growth and viability. *Mat. Sci.Eng. C* 76, 439–447 (2017). doi:
527 10.1016/j.msec.2017.03.063.
528 [35] Stöber W, Fink A, Controlled growth of monodisperse silica spheres in the micron
529 size range, *J. Colloid Interface Sci.* 26, 62–69 (1968).
530 [36] Miola M, Multari C, Debellis D, Laviano F, Gerbaldo R, Vernè E,
531 Magneto-plasmonic heterodimers: Evaluation of different synthesis approaches. *J Am*
532 *Ceram Soc.*1–10 (2021).
533 [37]Panagiota S, Louloudi M, Deligiannakis Y, EPR study of phenolic radical
534 stabilization by grafting on SiO_2. *Chemical Physics Letters* 472, 85-89 (2009) . Doi:
535 10.1016/j.cplett.2009.02.080
536 [38] Cheraghipour E, .Javadpour S, Mehdizadeh, AR, Citrate capped superparamagnetic
537 iron oxide nanoparticles used for hyperthermia therapy *J. Biomedical Science and*
538 *Engineering*, 5, 715-719 (2012). doi: 10.4236/jbise.2012.512089.
539 [39] Nigam S, Barick KC, Bahadur D. Development of citrate-stabilized Fe*3*O*4*
540 nanoparticles: Conjugation and release of doxorubicin for therapeutic applications a, *J.*
541 *Magn. Magn. Mat.* 323, 237–243 (2011). Doi: 10.1016/j.jmmm.2010.09.009
542 [40] Kulshrestha P, Gogoi M, Bahadur D, Banerjee R. In vitro application of paclitaxel
543 loaded magnetoliposomes for combined chemotherapy and hyperthermia. *Colloids Surf*
544 *B Biointerfaces* 96, 1-7(2012). doi: 10.1016/j.colsurfb.2012.02.029.
545 [41] Bini RA, Marques RFC, Santos FJ, Chaker JA, Jafelicci Jr M,. Synthesis and
546 functionalization of magnetite nanoparticles with different amino-functional

547 alkoxysilanes. *J. Magn. Magn. Mat.* 324, 534–539 (2012). Doi:
548 10.1016/j.jmmm.2011.08.035
549 [42] Khatiri R, Reyhani A, Mortazavi SZ, Hossainalipour M. Preparation and
550 characterization of Fe3O4 /SiO2 / APTES core-shell nanoparticles. Proceedings of the
551 4th *International Conference on Nanostructures*. (2012).
552 [43] Kanimozhi S, Perinbam K. Synthesis of amino-silane modified superparamagnetic
553 Fe3O4 nanoparticles and its application in immobilization of lipase from Pseudomonas
554 fluorescens Lp1. *Materials Research Bulletin*, 48, 1830-1836 (2013). Doi:
555 10.1016/j.materresbull.2013.01.024Get rights and content
556 [44] Wang W, Chen Q, Jiang C, Yang D, Liu X, Xu S, One-step synthesis of
557 biocompatible gold nanoparticles using gallic acid in the presence of poly-(N-vinyl-2-
558 pyrrolidone), *Colloids and Surfaces A: Physicochem. Eng. Aspects* 301, 73–79 (2007).
559 doi:10.1016/j.colsurfa.2006.12.037
560 [45] Deligiannakis Y, Sotiriou GA, Pratsinis SE. Antioxidant and Antiradical SiO2
561 Nanoparticles Covalently Functionalized with Gallic Acid. *ACS Appl. Mater. Interfaces*
562 4, 6609−6617 (2012). doi: 10.1021/am301751s.
563 [46] Nadeema K, Ali L, Gul I, Rizwand S, Mumtaz M, Effect of silica coating on the
564 structural, dielectric, and magnetic properties of maghemite nanoparticles. *J. Non-*
565 *Crystal. Sol.* 404, 72–77 (2014). Doi: 10.1016/j.jnoncrysol.2014.07.036
566 [47] Emadi M, Shams E, Kazem Amini M, Removal of Zinc from Aqueous Solutions
567 by Magnetite Silica Core-Shell Nanoparticles. Journal of Chemistry 2012, ID 787682
568 (2013). Doi: 10.1155/2013/787682

[48] Cheraghipour E, Javadpour S, Mehdizadeh AR, Citrate capped superparamagnetic iron oxide nanoparticles used for hyperthermia therapy, *J. Biomed. Sci. Eng.* 5, 715–719 (2012) . DOI: 10.4236/jbise.2012.512089.

[49] Cozzoli PD, Pellegrino T, Manna L, Synthesis, properties and perspectives of hybrid nanocrystal structures, *Chem. Soc. Rev*. 35, 1195–1208 (2006). Doi:10.1039/B517790C

[50] Goetze TC, GansauBuske N, Roeder M, Gornert P, Bahr M, Biocompatible magnetic core/shell nanoparticles, *J. Magn. Magn. Mater*. 252, 399–402 (2002). Doi:10.1016/S0304-8853(02)00624-8

[51] Campelj S, Makovec D, Drofenik M, Preparation and properties of water-based magnetic fluids, *J. Phys. Condens. Matter* 20, 204101 (2008). doi: 10.1088/0953-8984/20/20/204101 * One of the most significant examples of the use of citric acid as stabilizing and dispersant agent.

[52] Zeng H, Sun S. Syntheses, Properties, and Potential Applications of Multicomponent Magnetic Nanoparticles. *Adv. Func. Mat.* 18, 391-400 (2008). Doi: 10.1002/adfm.200701211 * Complete and detailed review concerning the development of multicomponent nanoparticles.

[53] Cham-Fai Leung K, Xuan S, Zhu X, et al.Gold and iron oxide hybrid nanocomposite materials. *Chem. Soc. Rev.* 41, 1911–1928(2013). Doi: 10.1039/C1CS15213K

Table of Contents graphic

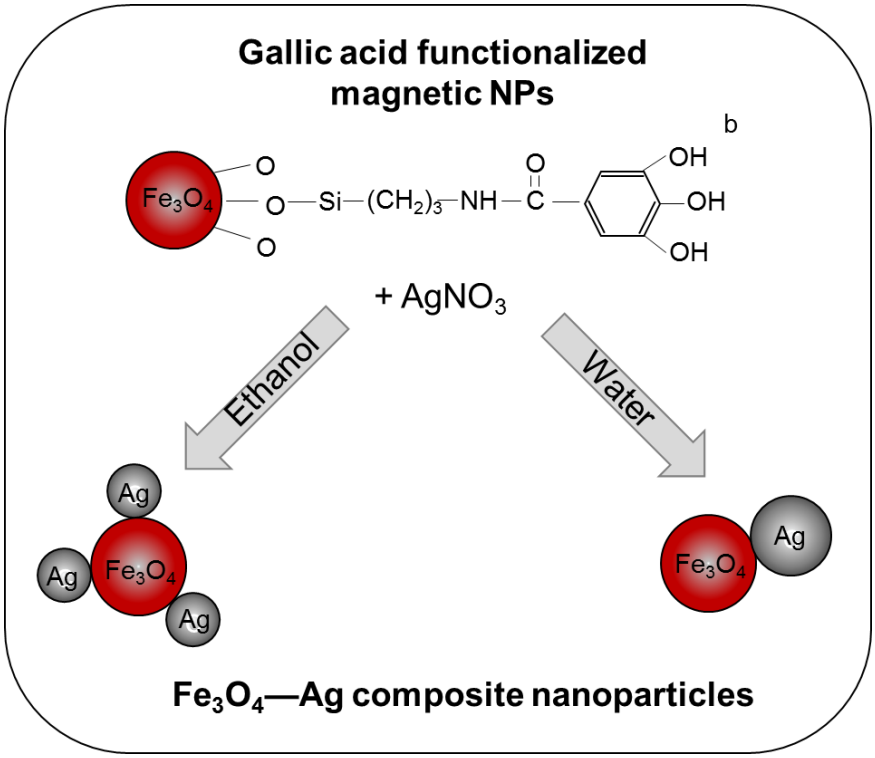
Gallic acid functionalized magnetic NPs
b
Fe3O4
O
O
O
Si
(CH2)3
NH
C
O
OH
OH
OH
+ AgNO3
Ethanol
Water
Ag
Ag
Fe3O4
Ag
Fe3O4
Ag
Fe3O4—Ag composite nanoparticles

591